2016 24th International Lightning Detection Conference &
6th International Lightning Meteorology Conference
18 - 21 April | San Diego, California, USA

GLD360 Upgrade: Performance Analysis and Applications

Ryan Said[1], Martin Murphy[1]
[1]Vaisala, Inc., Louisville, Colorado
ryan.said@vaisala.com

Abstract— **The Vaisala GLD360 global lightning dataset is generated by a long-range network that employs both Time of Arrival (TOA) and Magnetic Direction Finding (MDF) technologies at each sensor to geo-locate individual lightning flashes. The sensors, sensitive to the Very Low Frequency range (VLF; ~500 Hz—~50 kHz), use a waveform recognition algorithm to identify specific features in radio atmospherics generated by individual lightning discharges. A propagation correction is applied to the time delay of each feature in order to recover a more consistent arrival time across a wide range of distances and propagation conditions. An attenuation model is also applied to the amplitude of the waveform, which is used to recover an estimate of peak current.**

On August 18, 2015, Vaisala released an update to the location algorithm that generates the GLD360 dataset. This update includes several enhancements that are targeted at improving the performance of the network. The primary changes include a more refined propagation model, improved sensor correlation heuristics, and a more robust backend infrastructure. Using reprocessed and pre-update production data, an analysis of the network performance before and after the upgrade is given. Using lightning data from Vaisala's National Lightning Detection Network (NLDN) as a reference, quantitative validation results are presented that analyze the relative ground flash and cloud pulse detection efficiency, ground stroke location accuracy, and ground stroke peak current magnitude performance.

The global extent of the GLD360 dataset makes it well suited to a variety of meteorological and warning applications. The utility of the network in these types of applications is dependent on the data quality in the region of interest. We apply GLD360 data, reprocessed with the new algorithm, to two applications. First, we use a peak current filter to estimate annual ground flash density rates, using a single year of reprocessed data. Second, we provide a follow-up to previous studies that analyzed GLD360's skill as a lightning warning system, using the practical figures of merit of probability of detection and total duration in a warning state. This updated analysis of GLD360's utility as a lightning warning system is compared against the warning performance using lightning data from NLDN.

Keywords—lightning detection networks; GLD360; lightning climatology; lightning warning

I. INTRODUCTION

Long-range terrestrial lightning location systems (LLS) provide near real-time lightning data over continental-scale regions. Using receivers sensitive to the Very Low Frequency (VLF; 3–30 kHz) range, long-range LLS leverage efficient guiding in the Earth-ionosphere waveguide at these frequencies [Davies, 1990, p. 389] to measure radio impulses emitted from large current processes in individual lightning discharges at large (several thousand kilometer) distances. A central processor (CP) combines measurements from multiple sensors to calculate the time and location of the causative discharge. In many cases, this calculation estimates the quality of the solution and calculates additional properties of the discharge, including peak current and polarity [Said et al., 2010].

Long-range LLS usually have inferior performance across all relevant metrics compared to shorter-baseline networks, including a larger location accuracy (LA), lower flash detection efficiencies (DE), and, when available, less reliable peak current estimates [Nag et al. 2015]. The location accuracy for long-range lightning detection systems is typically an order-of-magnitude worse than shorter baseline networks with a higher sensor bandwidth. Given perfectly coherent detection, the limited frequency bandwidth of long-range LLS is not a theoretical impediment to sub-kilometer location accuracy [Lee 1989]. However, practical limitations, including variable propagation conditions, signal-to-noise ratio constraints, and uncorrected waveguide dispersion effects typically limit the LA of these systems to several kilometers. In addition, continental-scale networks preferentially detect cloud-to-ground (CG) return strokes and some inter- or intra-cloud (IC) discharges with large peak current amplitudes. In contrast, shorter baseline networks with sensor bandwidth extending through the Low Frequency (LF; 30–300 kHz) and Medium Frequency (MF; 300 kHz–3 MHz) range detect a larger fraction of both CG and IC flashes with a better spatial resolution, on the order of several hundred meters.

The performance of long-range networks is an important consideration to the applications that use the lightning data. Many of the same ground-truth validation techniques applied to national-scale VLF/LF networks can be equally applied to longer-range networks (see, for example, Mallick et al. [2014b, 2014c]). However, due to the longer baselines and more variable propagation conditions of the Earth-ionosphere waveguide, a careful examination of the spatial and temporal uniformity of these performance metrics is particularly important to a more complete evaluation of a long-range LLS. Inter-network comparisons between long-range LLS and higher performance regional LLS provide a means to evaluate the long-range LLS performance across wider regional and time domains. These comparative analyses provide relative performance metrics that necessarily depend on the quality of the reference network data. A more detailed discussion of the strengths and limitations between various network validation techniques is included in Nag et al. [2015] and references therein.

This paper evaluates multiple performance parameters of the GLD360 dataset, which is generated by a global lightning detection network owned and operated by Vaisala [Said et al. 2013]. GLD360 uses a waveform recognition algorithm to identify specific features in radio atmospherics generated by individual lightning discharges and to estimate polarity. A propagation correction is applied to the time delay of each waveform feature in order to reduce the arrival time error across a wide range of distances and propagation conditions. An attenuation model is also applied to the amplitude of the waveform, which is used to recover an estimate of peak current magnitude. The GLD360 network employs both Time of Arrival (TOA) and Magnetic Direction Finding (MDF) technologies at each sensor, which is unique among long-range LLS. GLD360 does not classify events between CG strokes and IC pulses; all events are labeled CG strokes.

On August 18, 2015 Vaisala released an upgrade to the network software behind the GLD360 dataset. This paper presents preliminary estimates of the resulting change in performance by comparing pre-upgrade production against reprocessed GLD360 data together with reference data from the National Lightning Detection Network (NLDN). The subsequent section applies the upgraded dataset to two specific applications: a direct estimate of global ground flash densities, and using GLD360 lightning data as a thunderstorm warning system.

II. Overview of GLD360 Update and Comparison with NLDN

The upgrade to the GLD360 network on August 18, 2015 included algorithm changes to the CP. A detailed description of these modifications is left to future work. The difference in performance due to processing changes at the CP can be quantified by comparing the production dataset before the upgrade date to data generated by reprocessed archived sensor data with the new algorithm. For this purpose, GLD360 sensor data from January 1, 2014 through the upgrade date has been reprocessed. In the calendar year 2014, the production GLD360 dataset reported 822 million strokes. Over the same time period, the reprocessed dataset contains 1,480 million strokes, an 80% increase.

In this section we use NLDN data as a reference to compare the performance of the production and reprocessed GLD360 dataset over CONUS. Events from July 1 through July 31, 2015 from both the production and reprocessed datasets are compared at the stroke level to NLDN Total Lightning (TL) data. Individual return strokes and cloud pulses are matched between the GLD360 (test) and NLDN (reference) datasets if the location and time of an event from each are within 50 km and 150 microseconds, respectively.

Fig. 1 shows the total flash density measured by NLDN and GLD360 over the one month analysis period. Note that the density values in Fig. 1 are scaled up to annual values, even though the data are from one month (July); these are not true annual flash densities. Strokes from each network were matched over the latitude range [30–48] degrees north and longitude range [125–75] degrees west, shown by the inner box in each plot. Over this analysis area, both networks observe similar spatial patterns of flash density. Given the install base of sensors over CONUS and Canada, NLDN's coverage extends ~250 km from the coastal boundary and southern border with Mexico [Nag et al., 2014]. However, the expected falloff in NLDN's DE with decreasing latitude into Mexico is clearly evident by comparing NLDN's total flash density with values reported by

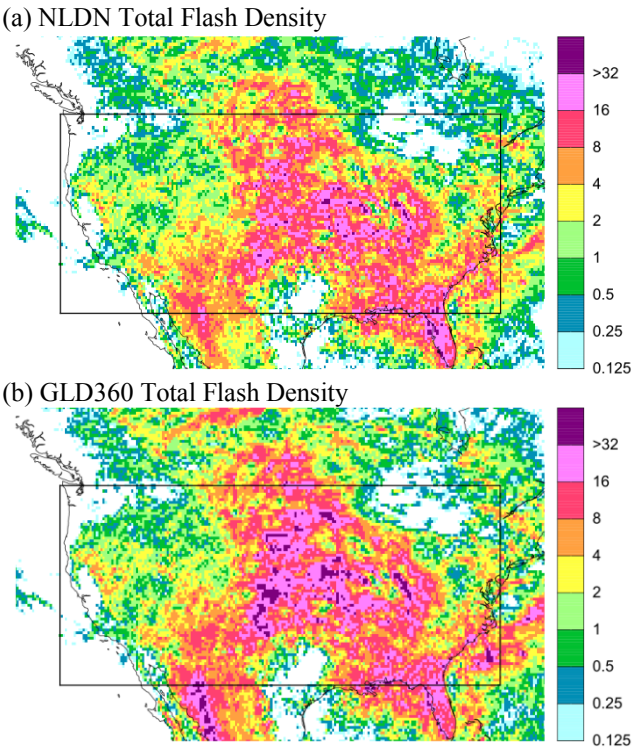

Fig. 1. Total flash density measured by NLDN (a) and GLD360 (b) for July 1 – July 31, 2015, given in fl-km^{-2}-yr^{-1}. Flash counts are summed in 0.5° x 0.5° bins and scaled to correspond to a flash density per year assuming the same average rate observed in July. The inner box indicates the comparison window used to derive the validation results presented in Section II.

the reprocessed GLD360 dataset. In the interior of CONUS, the total flash counts between the two networks generally track each other, usually within a factor of 2.

Fig. 2 evaluates the dependence of the relative DE on peak current and time of day. As shown in Fig. 2a, in both the production and reprocessed datasets, the ground flash DE decreases with decreasing peak current magnitude. However, the flash DE of the reprocessed dataset is higher compared to the production dataset for every peak current range. For large negative CG flashes, the reprocessed GLD360 dataset detects nearly every NLDN-reported CG flash; the relative CG flash DE is over 99% for negative peak current magnitudes above 45 kA, and above 90% for negative flashes larger than 17.5 kA. In contrast, the production dataset CG flash DE saturates at ~88% for large negative events. The increase in DE is larger for positive flashes. In the reprocessed dataset, the DE saturates at

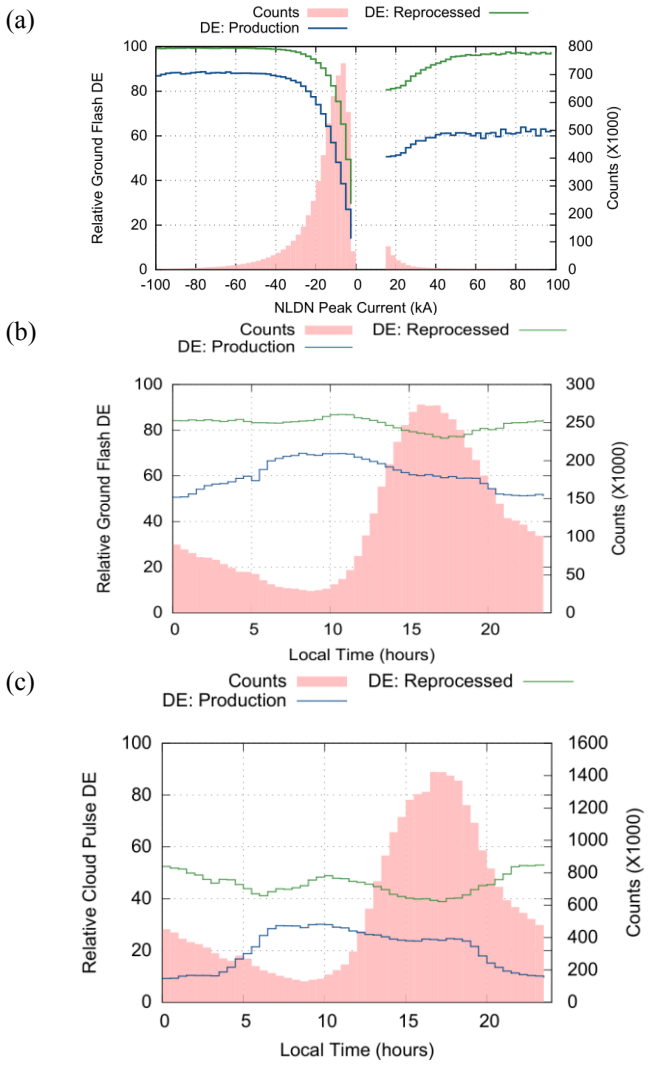

Fig. 2. Relative CG flash DE (a,b) and relative IC pulse DE (c) versus NLDN peak current (a) and local time (b, c). Relative DE of the pre-upgrade production dataset (blue) and the reprocessed dataset (green) are shown together with the number of NLDN flash or pulse counts (pink) for each peak current or local time range bin. Peak current bin widths are 2.5 kA; local time bin widths are 30 minutes.

~97% for large events, compared to ~60% in the production dataset. Integrated over all peak current bins, the total CG flash DE increased from 59% to 81%.

Figs. 2b and c show the diurnal dependence of the relative CG flash DE and cloud pulse DE with respect to local time, which is calculated using the time and longitude of the reference event. In both cases, the relative DE of the reprocessed dataset exhibits significantly less diurnal variation compared to the production dataset. The overall CG flash DE for the reprocessed dataset holds near 85% for the nighttime and early and late daytime hours. During the peak activity in the late local afternoon hours, the relative CG flash DE dips to 76%. This dip is correlated with the increase in total flash counts, rather than with a change in day/night ionospheric propagation profiles. Hence, the dip is likely caused by count saturation effects at the sensor and CP and not due to the diurnal dependence of propagation losses in the Earth-ionosphere waveguide. In contrast, the production relative CG flash DE varies between 50% and 70%, and is at a minimum during local midnight.

The reprocessed relative IC pulse DE shows a similar dip during the peak late afternoon thunderstorm hours. The reprocessed DE also exhibits a slight diurnal dependence, with a small increase in DE during the local nighttime hours. On average, nighttime ionospheric losses are lower, so the detection of weaker cloud pulses is expected to increase slightly for events detected over nighttime propagation paths. In contrast, the production dataset shows a sharp decrease in relative cloud pulse DE during the nighttime paths, as with the relative CG flash DE. Since the production and reprocessed datasets are derived using the same sensor data, this dip is not due to an underlying sensor detection issue. The relatively poor nighttime detection of IC pulses and, to a lesser extent, CG flashes in the old algorithm may instead be due to an oversimplified propagation correction algorithm for nighttime paths that prevented a high yield during the sensor correlation and quality control steps in the location algorithm.

Overall, the reprocessed dataset detected 44% of the cloud pulses reported by NLDN, compared to 21% detected by the production dataset. While the relative cloud pulse DE represents a conservative lower bound to the relative cloud flash DE, the <50% cloud pulse DE, combined with the similar total flash counts over the analysis window seen in Fig. 1, suggest GLD360 is uniquely detecting a significant fraction of flashes. A more complete characterization of these uniquely detected flashes is left to future work.

The limited spatial resolution offered by long-range lightning detection networks typically limit their use for energy applications [Borghetti et al. 2006]. Thus, peak current estimates have limited practical use in such networks. However, in the next section we use peak current as a crude averaged proxy for source type classification. To justify this approach, in this section we evaluate the relative peak current magnitude error using NLDN ground strokes as a reference. Fig. 3 shows the geometric mean of the peak current magnitude error versus NLDN peak current and local time. In both the production and

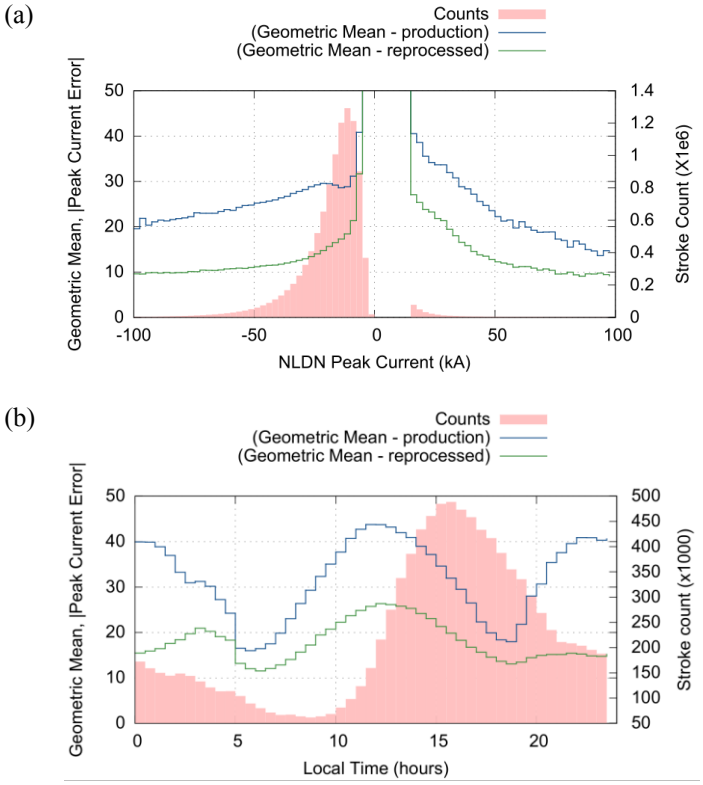

Fig. 3. Relative peak current magnitude error for CG strokes versus NLDN ground stroke peak current (a) and local time (b). Peak current error of the production (blue) and reprocessed (green) datasets are shown together with the number of NLDN ground strokes in each peak current or local time bin (pink). Peak current bin widths are 2.5 kA; local time bin widths are 30 minutes.

reprocessed datasets, the fractional error decreases with increasing amplitude. The peak current error of the reprocessed dataset is roughly half as large as the production dataset. This reduction by approximately a factor of two in the relative error is also evident in the plot against local time. In the reprocessed dataset, the relative error is ~10–12% during the nighttime hours, rises to 20% just before sunrise, and then slowly rises from ~10 to ~25% between sunrise and local noon, before falling back to ~10% at sunset. The symmetric pattern in the daytime peak current error profile follows the elevation angle of the sun at the solution location. The new propagation algorithm does not include additional daytime propagation correction factors that account for the sun elevation angle. This plot suggests that introducing additional correction factors that account for sun elevation could reduce the daytime peak current error by over a factor of two. The larger peak current error at sunrise compared to sunset suggests the day/night propagation correction is less robust during the sunrise ionospheric transition. A detailed exploration of this asymmetry would need to account for mode coupling effects between the daytime and nighttime propagation conditions and is left to future work.

Fig. 4 shows the histogram and cumulative distribution function (CDF) of the relative location error for both the production and reprocessed datasets. Adjustments to the waveform identification scheme, improvements to the propagation correction parameters, and other modifications to

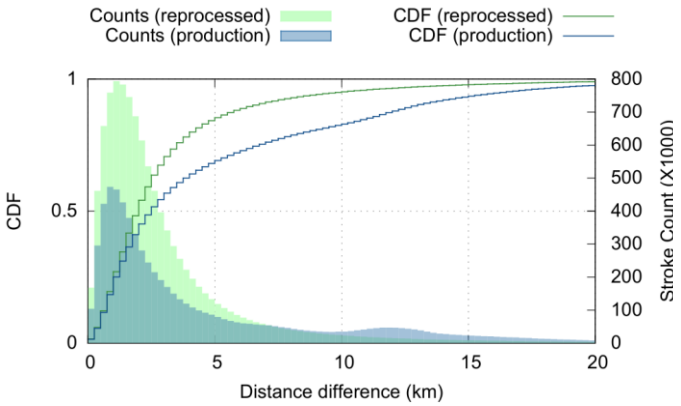

Fig. 4. Histogram and cumulative distribution function of the relative ground stroke location error between NLDN CG strokes and matched events from the production (blue) and reprocessed (green) datasets.

the location algorithm improved the median location accuracy from 2.4 km to 1.8 km, and the 90th percentile location error from 12.9 km to 6.4 km. The reduction in large-error outliers should benefit the second class of applications considered below, lightning warning systems.

This inter-network comparison does not provide an absolute reference for GLD360's performance, since the results are dependent on the accuracy and completeness of NLDN's lightning data. NLDN's CG flash DE, stroke LA, and peak current error have been well characterized and validated in the literature. Using rocket-triggered lightning data at a facility in Camp Blanding, Florida as ground truth, Mallick et al. [2014a] validate multiple NLDN CG flash performance parameters. In the most recent year evaluated (2013), they report the LA to be better than 200 m, a CG flash DE >95%, and a peak current magnitude error of 15%. Given the high ground flash DE and order-of-magnitude better LA, it is assumed in this analysis that the NLDN CG flash data is ground truth (100% flash DE, exact return stroke location). In contrast, we treat the relative cloud pulse DE as a qualitative result. NLDN's cloud flash DE is lower than the CG flash DE (50–60% [Murphy and Nag, 2015]), and there is no means to provide an absolute cloud pulse reference. In addition, the peak current error of the reprocessed dataset is of the same order of magnitude as the absolute peak current error for NLDN subsequent strokes, so an additional error term is needed to properly characterize the results shown in Fig. 3.

III. Applications

A. Ground Flash Density

The first application we consider is an estimate of annual CG flash density, a parameter of particular importance in lightning protection and electric power applications. We use the reprocessed GLD360 data from the calendar year 2014, and we preferentially isolate the CG flashes by applying a peak current-based filter.

As a reference, Fig. 5a shows the total flash density from Fig. 2a of Cecil et al. [2014a], redrawn here using HRFC_COM_FR grid data from Cecil et al. [2014b] with the same color scale as the GLD360-derived flash density plots

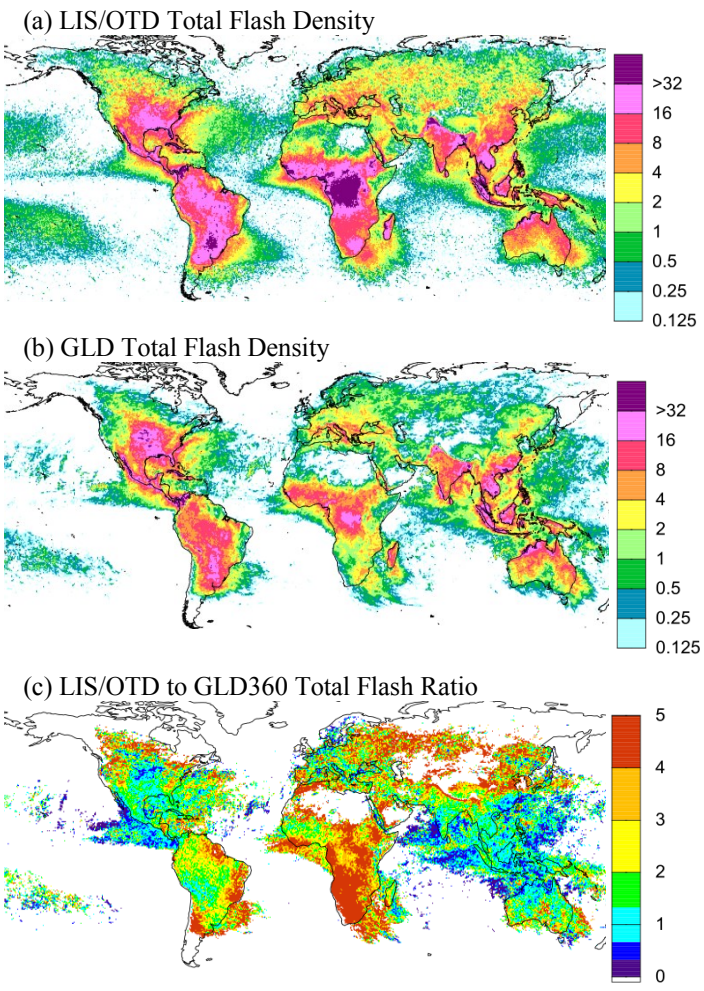

Fig. 5. (a) LIS/OTD total flash density (fl-km^{-2}-yr^{-1}) composite on a 0.5^{o} x 0.5^{o} grid. (b) GLD360-determined total flash density using reprocessed 2014 data, shown with the same color scale and grid size. (c) Ratio between flash densities shown in (a) and (b), shown for pixels where the GLD360-determined total flash density is greater than 0.25 fl-km^{-2}-yr^{-1}.

shown in Fig. 5b. This total flash density plot is generated using 15 years of spaceborne optical observations from the Optical Transient Detector (OTD) and Lightning Imaging Sensor (LIS), and represents the current best estimate of the absolute annual total flash density. Fig. 5b shows the reprocessed total flash density reported by GLD360, where no peak current-based filtering has been applied. The GLD360 flash density is derived by grouping strokes into flashes using a 1-second, 15-km window. The flash density is calculated on a 0.5^{o} latitude/longitude grid, where the total counts in each bin are normalized by the latitude-dependent area of the pixel.

Since the color scale saturates at 32 fl-km^{-2}-yr^{-1}, Figs. 5a and 5b de-emphasize the difference between the LIS/OTD and GLD360 total flash density estimates in areas with very high annual flash rates. For example, Cecil et al [2014a] note a maximum annual flash rate of 160 fl-km^{-2}-yr^{-1} in Eastern Congo, which is a factor of 5 larger than the highest color scale value in Figs. 5a and 5b. Fig. 5c plots the ratio between the flash densities shown in Figs. 5a and 5b. The ratio color scale saturates at 5; any ratio higher than 5 is plotted in red.

Over much of the Americas, Europe, Southeast Asia, and Australia, the total flash density ratio is at or below 2. This relative equivalence in annual total flash densities suggests that GLD360's total flash DE is on the order of 50% or higher over these geographic regions. In some of the oceanic pixels in Southeast Asia, GLD360's flash density is over 50% larger than the 15-year LIS/OTD lightning climatology (where the ratio is less than 2/3). This plot also highlights areas where the DE is much lower. GLD360's decreasing DE over Africa, Argentina, and eastern Brazil are clearly evident in this plot. Curiously, the ratio contains a local peak along a trace just south of the Himalayan mountain region, a pattern that warrants further study.

Many of the high spatial frequency artifacts in Fig. 5c are undoubtedly due to single-year weather patterns. In particular, there are many 0.5^{o} pixels in Canada and Siberia where the ratio is 3 or higher in close proximity to many lower ratio regions. These high-latitude areas are characterized both by low absolute flash counts and smaller pixel sizes by area. Hence, we expect deviations in individual weather patterns from 2014 compared to longer-term averages to lead to rapid spatial changes of the ratio.

To estimate the annual ground flash density, the flash dataset shown in Fig. 5b is passed through a peak current magnitude filter, which removes all flashes with a peak current magnitude less than I_{min}. In the stroke-to-flash grouping algorithm used in this study, the largest amplitude constituent stroke determines the peak current of the overall flash. The threshold I_{min} is chosen such that the contribution from cloud flashes is insignificant compared to overall CG flash counts. Using NLDN data, Nag et al. [2015] found a negligible contribution of effective peak currents from IC pulses above 30 kA for both positive and negative events; above this threshold, the overall counts are dominated by CG activity. Here, we show the results with threshold I_{min} = 30 kA and 40 kA. After either threshold is applied, the flash density is recalculated and then scaled using the CG flash peak current distribution based on the log-normal fit to tower measurements shown in Berger [1975]. According to this log-normal fit, truncating the GLD360 flash data using I_{min} = 30 kA and 40 kA removes 50% and 70% of the negative ground flash population, respectively. Thus, for these two thresholds, we scale the ground flash density estimate by 1/0.5 and 1/0.3, respectively.

Figs. 6a and b show the resulting CG flash density estimates using the 30 kA and 40 kA thresholds, respectively. These estimates of CG flash density include several assumptions with varying degrees of uncertainty about the underlying peak current distributions of natural lightning and the network performance. Firstly, the CG flash peak current distribution is assumed to be the same for all regions across the globe and equal to the negative CG flash distribution given in Berger et al [1975]. We also assume the CG flash DE is geographically and temporally constant, and we apply no DE adjustment above I_{min} (i.e., we

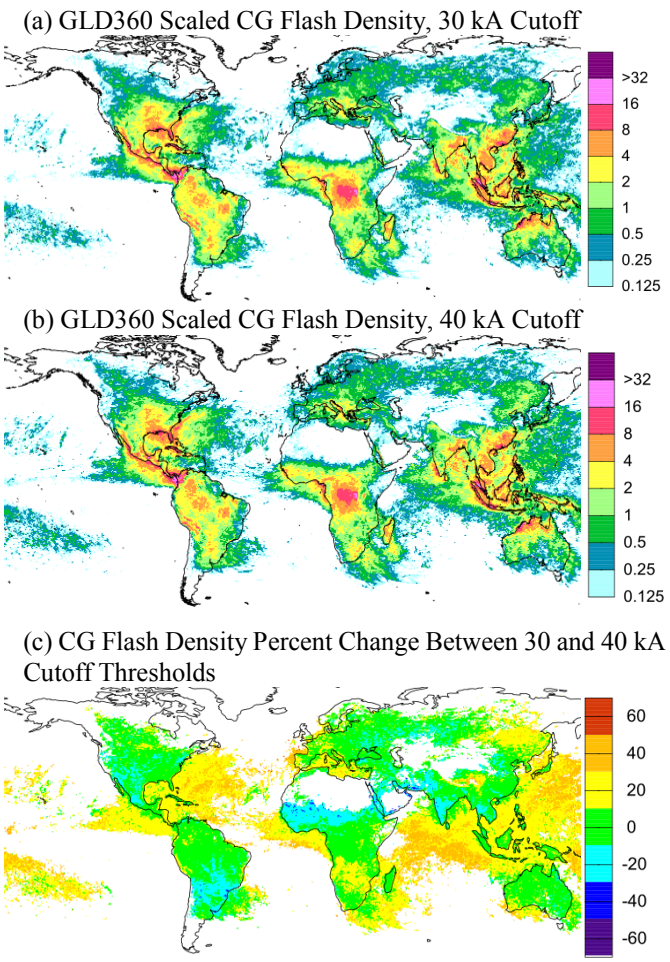

Fig. 6. (a,b) Scaled GLD360-determined CG flash density estimate (fl-km^{-2}-yr^{-1}) using a 30 kA cutoff (a) and a 40 kA cutoff (b). (c) Percent change of GLD360 ground flash density estimate using the 40 kA cutoff compared to a 30 kA cutoff. Pixels where the 30 kA ground flash density is less than 0.125 fl-km^{-2}-yr^{-1} are not shown. All thematic map plots shown with 0.5^{o} x 0.5^{o} resolution.

assume 100% CG Flash DE). In addition, the GLD360 peak current estimates are assumed to be accurate and temporally and geographically stable; no diurnal or spatially-dependent peak current correction factor is applied before the dataset is filtered by I_{min}.

The sensitivity of the CG flash density estimate to I_{min} reflects the combination of all of the error terms corresponding to each of these underlying assumptions. Fig. 6c shows the percent change in CG flash density estimate of the 40 kA threshold compared to the 30 kA threshold. For the vast majority of pixels, the CG flash density estimate varies by less than 30%. Regions where the 40 kA threshold yields a density estimate between 10–30% less than the 30 kA threshold are largely restricted to land masses; the 10–30% higher estimate pixels are dominated by oceanic regions.

The year-long flash density measurement averages over the diurnal variations of peak current error shown in Fig. 3, and anyway, peak current errors are at most about 20%. Regional differences are therefore likely dominated by a combination of variations in both DE and the natural CG flash peak current distribution. As mentioned above, we have not applied any DE-based correction factors, effectively assuming the CG flash DE is 100% above I_{min}. In reality, the CG flash DE is lower, and so we are missing a DE correction factor α_{DE}, where $\alpha_{DE} > 1$. If we assume that the CG flash DE is a monotonically increasing function with peak current magnitude, as observed in Fig. 2a, applying a higher I_{min} to the CG density calculation will decrease α_{DE} proportionally more in regions with lower DE compared to regions with higher DE. Hence areas with lower overall CG flash DE would show a relative increase in the CG flash density estimate for higher values of I_{min}. This effect is convolved with CG density estimate errors due to variations and uncertainty in the underlying CG flash peak current distribution. If the distribution is shifted to higher peak current magnitudes compared to the assumed distribution, then the CG flash density estimate should be scaled by a factor α_{IP}, where $\alpha_{IP} < 1$. Given a log-normal distribution, this additional correction factor decreases with increasing values of I_{min}. Hence, if the underlying CG peak current distribution is skewed higher, then increasing I_{min} will increase the overestimate of the CG flash density. Thus, regions in Fig. 6c with a higher relative estimate could also correspond to regions with a peak current magnitude distribution skewed to higher values.

We suggest that the variation in the CG flash density estimate between the two peak current thresholds shown in Fig. 6c is dominated by variation in the natural CG flash peak current distribution. The transition between the light blue (10–30% lower estimate), green (within 10% difference), and yellow (10–30% higher estimate) generally follow terrain patterns with a high spatial frequency, instead of slow transitions in the interior of more sparsely covered oceanic regions. The apparent trend to higher peak current magnitude distribution in the oceans, in particular, is consistent with past studies that show a skew to higher effective peak currents reported by ground-based LLS over the oceanic regions (see, for example, Said et al. [2013] and references therein).

B. Warning Analysis

In this section we evaluate the effectiveness of the reprocessed GLD360 dataset as an operational CG lightning warning system. A measure of the skill of a lightning warning system typically consists of three metrics: the probability that a storm will be detected with sufficient advanced warning to take precautionary actions, the false alarm ratio, and the total time spent in a warning state. The first metric addresses safety. If a storm that eventually produces a CG strike in an Area of Concern (AOC) is detected before the first CG strike occurs, there is an opportunity to protect ground assets and personnel. The latter two metrics are measures of efficiency. The longer a warning system is in an alert state, and the more often it is unnecessarily in an alert state, the more cost is accrued due to stalled ground operations. Several past studies have analyzed the effectiveness of LLS as CG warning systems [Murphy and Holle, 2006; Holle and Demetriades 2010; Holle et al 2014]. This analysis uses the same methodological approach as these

earlier studies to evaluate the relative warning skill using the reprocessed GLD360 dataset in comparison to the higher-resolution NLDN dataset.

Using the methodology detailed in Holle et al. [2014], we evaluate the probability of detecting the first CG stroke of a storm in an AOC with at least a two minute lead time (POD2), and the percent time spent in a warning state. NLDN CG flash data is used as ground truth for the existence of a CG stroke in the AOC. Lightning activity over a larger warning area (WA) that encompasses the AOC triggers an alert state. The alert state remains active until 15 minutes past the last lightning event of a storm in the WA. The results below separately evaluate NLDN TL and GLD360 as the data source for these WA triggers.

This study includes 11 airports as hypothetical warning areas throughout the Midwest and South, and analyzes data from June 1, 2014 through August 31, 2014, a duration of 132,480 minutes. The airports included are Atlanta, Charlotte, Dallas-Fort Worth, Houston, Kansas City, Nashville, New Orleans, Oklahoma City, Orlando, San Antonio, and St Louis. The AOC is defined as a circle with a 2.0 km radius. The WA is defined as a circle with the same center as the AOC. In order to establish a trend and provide greater insight on the relative performance of each network, we evaluate three separate WA radii: 5, 7.5, and 10 km.

Fig. 7a shows the total warning duration for each network (NLDN versus reprocessed GLD360), for each of the 11 airports for the 10 km WA radius. Airports 10 (Orlando) and 11 (New Orleans) have the highest total warning duration. Fig. 7b shows the average percent time spent in a warning state per airport as a function of WA radius. Given the relatively large warning duration in Orlando and New Orleans, the average percent time is disproportionately influenced by these two locations. For each WA radius, the average time of each network is within 0.1%, or ~132 minutes.

Fig. 8a quantifies the POD2 for each airport using the 10 km WA radius, and shows the average POD2 across all airports as a function of WA radius. As seen by the linear regression lines in Fig. 8b, the POD2 for GLD360 is ~5% lower for each radius. Hence, to achieve the same POD2 with the GLD360 dataset, a larger WA radius should be used.

IV. Summary and Conclusions

This paper provides an initial analysis of the performance of the GLD360 network after the software upgrade released on August 18th, 2015. Using one month of NLDN data as a reference, multiple performance metrics were evaluated using both production and reprocessed GLD360 data. The relative CG flash DE increased from ~55–75% to ~75–85% depending on the local time of day, where the low end is likely caused by count saturation effects during peak thunderstorm activity rather than network sensitivity limitations. The relative IC pulse DE increased from ~10–30% to ~40–50%. Of the 80% overall increase in GLD360 event counts as a result of the algorithm upgrade, there was roughly a 30% increase in CG flashes (and thus, perhaps ~50% increase in CG strokes). There was also a doubling, approximately, in IC pulses; these comprise the remainder of the overall increase in counts (taking into account the naturally lower DE of IC pulses). The GM of the relative peak current magnitude error is reduced by a factor of 2, exhibits a diurnal variation, and asymptotically approaches 10% for the largest peak current magnitudes. The median location accuracy decreased from 2.4 km to 1.8 km, and the 90th percentile decreased from 12.9 km to 6.4 km.

(a) Total Time in Warning State

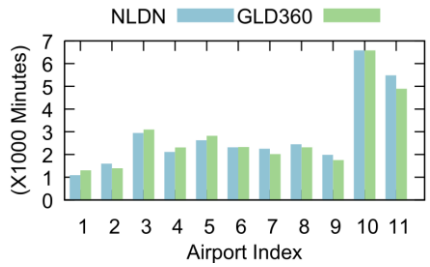

(b) Avg Percent Time in Warning State

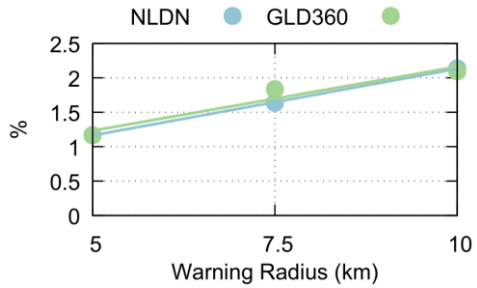

Fig. 7. (a) Total warning duration (in minutes) for each of the 11 airports in the study using a 10 km WA radius. (b) Average percent time spent in a warning state per airport versus WA radius.

(a)

(b)

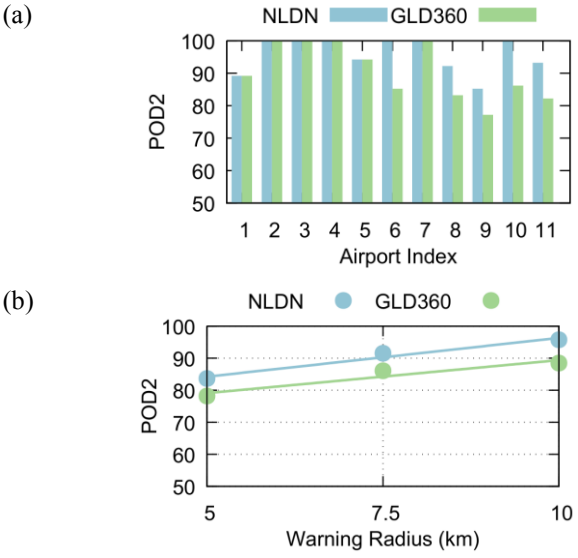

Fig. 8. (a) POD2 for the 10 km WA radius. (b) Average POD2 versus WA radius.

Two applications were considered using GLD360 data reprocessed with the new location algorithm. By clustering events into flashes and applying a suitably high peak current filter, an annual global ground flash density estimate was made using data from Jan 1, 2014–Dec 31, 2014. Finally, the lightning warning skill of reprocessed GLD360 data was compared against using NLDN data. For a given warning radius, the total warning duration across both networks was roughly equivalent, but the probability of detection with at least 2 minutes lead time was found to be ~5% higher using NLDN data.

REFERENCES

Davies, K. (1990), Ionospheric radio. No. 31. IET,

Berger, K. (1975), Parameters of lightning flashes, Electra 41: 23-37.

Borghetti, A., et al., (2006), A statistical approach for estimating the correlation between lightning and faults in power distribution systems, Probabilistic Methods Applied to Power Systems, 2006. PMAPS 2006. International Conference on. IEEE

Cecil, D. J. et al., (2014a), Gridded lightning climatology from TRMM-LIS and OTD: Dataset description, Atmospheric Research 135: 404-414.

Cecil, D.J., et al. (2014b), LIS/OTD Gridded Lightning Climatology Data Sets. Data set available online [https://ghrc.nsstc.nasa.gov/pub/lis/climatology/LIS-OTD/HRFC/] from the NASA Global Hydrology Resource Center DAAC, Huntsville, Alabama, U.S.A. doi: https://dx.doi.org/10.5067/LIS/LIS-OTD/DATA302

Cummins, K. L., and M. J. Murphy. (2009), An overview of lightning locating systems: History, techniques, and data uses, with an in-depth look at the US NLDN, Electromagnetic Compatibility, IEEE Transactions on 51.3: 499-518.

Holle, R. L., and N. WS Demetriades. (2010), GLD360 airport lightning warnings, 3rd Intl. Lightning Meteorology Conf., Vaisala, Orlando, Fla..

Holle, R. L., et al. (2014), Lightning warnings with NLDN cloud and cloud-to-ground lightning data, Lightning Protection (ICLP), 2014 International Conference of. IEEE.

Lee, A. CL. (1989), The limiting accuracy of long wavelength lightning flash location, Journal of Atmospheric and Oceanic Technology 6.1 (1989): 43-49.

Mallick, S., et al. (2014a), An update on the performance characteristics of the NLDN, 23rd International Lightning Detection Conference & 5th International Lightning Meteorology Conference.

Mallick, S., et al. (2014b), Evaluation of the GLD360 performance characteristics using rocket-and-wire triggered lightning data, Geophysical Research Letters41.10: 3636-3642.

Mallick, S., et al. (2014c), Evaluation of the WWLLN performance characteristics using rocket-triggered lightning data, Intl. Conf. on Grounding and Earthing/6th Intl. Conf. on Lightning Physics and Effects.

Murphy, M. and A. Nag, (2015) Cloud Lightning Performance and Climatology of the U.S. Based on the Upgraded U.S. National Lightning Detection Network, AMS Conference, Phoenix, AZ

Murphy, M., and R. L. Holle. (2006) Warnings of cloud-to-ground lightning hazard based on combinations of lightning detection and radar information." 19th International Lightning Detection Conference, Tucson, Arizona, USA.

Nag, A., et al. (2014), Recent evolution of the US National Lightning Detection Network. Preprints, 23rd Int. Lightning Detection Conf., Tucson, AZ, Vaisala.

Nag, A., et al. (2015), Lightning locating systems: Insights on characteristics and validation techniques. Earth and Space Science 2.4 65-93.

Said, R. K., et al., (2010), Long-range lightning geolocation using a VLF radio atmospheric waveform bank, Journal of Geophysical Research: Atmospheres 115.D23.

Said, R. K., et al., (2013), Highly intense lightning over the oceans: Estimated peak currents from global GLD360 observations, Journal of Geophysical Research: Atmospheres 118.13 6905-6915.